



Research Paper

Controllable synthesis of mesoporous cobalt oxide for peroxide free catalytic epoxidation of alkenes under aerobic conditions



Chandima Weerakkody, Sourav Biswas, Wenqiao Song, Junkai He, Niluka Wasalathanthri, Shanka Dissanayake, David A. Kriz, Biswanath Dutta, Steven L. Suib*

Department of Chemistry and Institute of Materials Science, University of Connecticut, 55 North Eagleville Road, U-3060, Storrs, CT 06269, United States

ARTICLE INFO

Keywords:

Alkene
Epoxidation
Heterogeneous
Cobalt oxide
Mesoporous

ABSTRACT

We report the synthesis of mesoporous Co_3O_4 by an inverse micelle template self-assembly method and its catalytic activity towards selective oxidation of alkenes to epoxides. The chemical and structural properties of the materials were characterized by powder X-ray diffraction, nitrogen sorption studies, electron microscopy, Raman spectroscopy, X-ray photoelectron spectroscopy and thermogravimetric analysis. The morphology of the material exhibits flower like nanoparticle aggregates. Nanoparticles are packed closely in a random manner to form the mesoporous network via connected interparticle voids. Particle size expansion could be observed with heat treatment (250 °C–450 °C), which strongly correlates with surface area of the material. Co-250, which has the highest surface area along with highest oxygen vacancies, gave the best performance in alkene epoxidation. The catalyst was found to be efficient in selective oxidation of alkenes to epoxides with a broad substrate scope and achieved > 99% conversion with high selectivity (93%). Liquid phase batch mode reactions were carried out under atmospheric pressure and aerobic conditions, in the absence of any additives. Moreover the catalyst could be recycled several times without losing its activity, which makes this catalyst economical and environmentally benign.

1. Introduction

Heterogeneously catalyzed aerobic oxidation of organic compounds has gained a great deal of attention due to its environmentally friendly nature and capability of use in large scale industrial synthesis [1,2]. Epoxidation of alkenes is a popular catalytic oxidation reaction, as epoxide products are expedient and vital intermediates in chemical and pharmaceutical industries [3]. Epoxides are considered as starting materials for various organic products including glycols, alcohols, carbonyl compounds, alkanolamines and polymers such as epoxy resins [4]. Epoxides are conventionally produced by either dehydrochlorination of styrene chlorohydrin with a base or oxidation of styrene using organic peracids. The conventional method for epoxidation of alkenes is being replaced by the method involving H_2O_2 or organic hydroperoxides as sacrificial oxidizing agents [5]. However, either poor selectivity or low styrene conversion has been observed when they were used as oxidizing agents [6]. Widely used homogeneous catalytic systems require expensive methods for product isolation and catalyst removal and are also considered as environmentally hazardous [7,8]. Use of heterogeneous catalysts for epoxidation reactions provides several advantages such as mild reaction conditions, ease of product isolation

and most importantly reusability and stability of the catalyst. Silver containing catalysts have been identified as the most efficient catalysts for gas phase epoxidation [9]. Other catalytic systems in this regard involve $\text{WO}_2(\text{acac})_2$ [10], organically modified Ti-MCM-41 [11], Au supported metal oxides [6,12,13], WO_2 [14], ferrierite [15], CuO [16], Ga-Co-HMS-X [17], titanium silicate [18], and hydrotalcites [19]. In spite of high activity and selectivity, most of the systems either use precious metals or are considered hazardous due to the use of peroxides to initiate the reaction. In addition, in some cases very low selectivity towards epoxides has been observed due to the formation of aldehyde byproducts [20]. In this context, cobalt containing systems have been identified as more active low cost materials. For example, Sun et al. [21] reported Co^{2+} Schiff complex supported on mesoporous silica and Tang et al. [22] reported Co^{2+} exchanged ZSM-5. However, addition of oxidizing agents such as tertiary butyl hydroperoxide (TBHP) was required to achieve higher conversion. Therefore, performing the reaction under aerobic conditions without any peroxide agents is a great challenge in catalytic epoxidation.

Tricobalt tetroxide is a well known heterogeneous catalyst for partial oxidation and surface reactions [23]. Spinel Co_3O_4 is considered as the most thermodynamically stable form among all cobalt oxides. This

* Corresponding author.

E-mail address: steven.suib@uconn.edu (S.L. Suib).

<http://dx.doi.org/10.1016/j.apcatb.2017.09.053>

Received 8 December 2016; Received in revised form 4 July 2017; Accepted 22 September 2017

Available online 23 September 2017

0926-3373/ © 2017 Elsevier B.V. All rights reserved.

structure contains Co^{3+} and Co^{2+} ions occupying octahedral and tetrahedral sites respectively [24,25]. Close thermodynamic stabilities of Co^{3+} and Co^{2+} play a major role in the redox chemistry of Co_3O_4 , as they can be interconverted at a significant rate on single crystal surfaces [23]. Among transition metal oxides, Co_3O_4 is well known for the presence of mobile oxygen, and thus is more reactive towards oxidation reactions [26]. Co_3O_4 also has excellent ability to bind and activate molecular oxygen to produce peroxy and superoxy radical species, which can easily initiate epoxidation types of reactions [20].

Mesoporous materials have attracted much attention in heterogeneous catalysis due to their higher performance in a wide range of applications. Higher surface area of mesoporous materials provides higher numbers of active sites per unit mass, exhibiting superior activity compared to their non porous analogues [27–30]. Reduced mass transfer limitations provide an added advantage, which allows higher adsorption of the substrate on the catalytic surface [31]. Furthermore, the diffusion of reactants could be facilitated by adjusting the size and the nature of the pores. For instance, attempts have been made to introduce an additional mesoporous structure into the microporous network to achieve such a goal [32]. Our group recently developed a class of mesoporous materials named UCT (University of Connecticut) materials, which gained much attention as the method leads to produce a series of metal oxides from different parts of the periodic table [33]. This method also allows synthesis of a metal oxide with different structural properties using a single synthetic scheme by varying the synthetic conditions [2,31,34–36]. Members of this group (meso Cs-MnOx [2,36], meso Mn_2O_3 [37]) are identified as quite efficient catalysts for versatile organic transformations with excellent reusability, therefore making UCT materials a new class of environmental friendly oxidation catalysts. Mesoporous UCT Co_3O_4 displayed superior activity over the commercial Co_3O_4 material in gas phase CO oxidation and H_2S adsorption [38,39]. In this work we attempt to achieve high conversion and selectivity of alkenes to epoxides, with no assistance of any sacrificial oxidizing agent (peroxides). Mesoporous UCT Co_3O_4 and alkene were mixed with the solvent (dimethylformamide) and the mixture was bubbled with atmospheric air at a rate of 10 mL/min. Use of air as terminal oxidant, avoidance of additives, low catalyst loading, and high reusability of the catalyst make this approach more desirable from both economical and environmental standpoints.

2. Experimental section

2.1. Synthesis of mesoporous Co_3O_4

In a typical synthesis 5 g (0.017 mol) of $\text{Co}(\text{NO}_3)_2 \cdot 6\text{H}_2\text{O}$ was dissolved in a solution containing 17 g (0.33 mol) of 1-butanol, 2.4 g (0.038 mol) of HNO_3 and 2.5 g (4.31×10^{-4} mol) of P123 surfactant in a 200 mL beaker under magnetic stirring at room temperature. The obtained clear gel was placed in an oven at 200 °C for 3.5 h. The obtained powder was washed with ethanol several times and dried in a vacuum oven overnight. Then the powder was calcined at 150 °C for 12 h and was further subjected to different calcination cycles at 250, 350 and 450 °C to achieve desired pore size and crystal structure. All the heating cycles were carried out under air and samples were named according to their calcination temperature as Co-X (X = 150, 250, 350 and 450 °C).

2.2. Catalyst characterization

The crystalline phase of the as synthesized materials were analyzed by powder X-ray diffraction (PXRD) using a Rigaku Ultima IV diffractometer ($\text{Cu K}\alpha$ radiation, $\lambda = 1.5406 \text{ \AA}$). The operating voltage and current were 40 kV and 44 mA respectively. The low angle PXRD patterns were collected in the 2θ range of 0.5–5° (scan rate = $0.5^\circ \text{ min}^{-1}$) whereas the wide angle PXRD patterns were collected over a 5–75° 2θ range (scan rate = 2° min^{-1}). Nitrogen

adsorption/desorption experiments were carried out using a Quantachrome Autosorb-1-1C automated adsorption system. Brunauer-Emmett-Teller (BET) and Barrett-Joyner-Halenda (BJH) methods were employed in order to determine the surface area and pore structure of the catalyst respectively. For the surface morphology study, a field emission scanning electron microscopy (FE-SEM) technique was used on Zeiss DSM 982 Gemini instrument with a Schottky emitter at an accelerating voltage of 2.0 kV having 1.0 mA beam current. In order to further investigate the detailed surface morphology of the catalyst, high-resolution transmission electron microscopy (HR-TEM) was performed on a JOEL 2010 UHR FastEM instrument with operating voltage of 200 kV. A suspension of catalyst was mounted on a carbon coated copper grid to prepare the samples. Raman spectra of the cobalt oxide materials were collected on a Renishaw 2000 Raman microscope with an Ar^+ ion laser (514 nm) as the excitation source. The thermogravimetric analysis (TGA) was performed using a TG 209 F1 Libra instrument coupled to a QMS 403C quadrupole mass spectrometer (TG-MS), in order to determine the thermal stability and surface adsorbed groups on the catalyst. Measurements were performed in the temperature range between 25 and 800 °C at a ramping rate of $10^\circ \text{C min}^{-1}$ in an air atmosphere.

2.3. Catalytic tests

2.3.1. Epoxidation of alkenes

In a typical epoxidation reaction, a mixture of 3 mmol of alkene, 10 mg of catalyst and 5 mL of dimethylformamide (DMF) was added to a 25 mL two neck round bottom flask equipped with a reflux condenser. The reaction mixture was heated to the desired temperature under stirring (700 rpm). Airflow was introduced in to the system by bubbling air at a constant rate (10 mL/min). After the reaction, the mixture was cooled to the room temperature and catalyst was filtered off. Most of the reactions were repeated twice and the average value was reported.

2.3.2. Analysis of reaction products

Gas chromatography mass spectrometry (GCMS) was performed with a 7820 GC system connected to a 5975 series MSD mass detector. An Agilent Technologies and nonpolar cross-linked methyl siloxane column (12 in \times 0.200 mm \times 0.33 μm) was used.

3. Results

3.1. Structural characterization of mesoporous Co_3O_4

3.1.1. Powder X-ray diffraction (PXRD)

Both the low angle (0.5–5°) and wide angle (5–75°) diffraction patterns for cobalt oxide materials, calcined at different temperatures (150, 250, 350 and 450 °C) are given in Fig. 1. Calcination was done at different temperatures in order to obtain a catalyst with varied surface area, pore volume, and pore diameter. All the materials except Co-150 gave wide angle diffraction lines corresponding to spinel Co_3O_4 and could be well indexed with the JCPDS database which certifies the absence of any other bulk crystalline phases. Wide angle PXRD lines for Co-150 could be assigned for the mixed phase of Co_3O_4 and $\text{C}_4\text{H}_6\text{CoO}_4 \cdot 4\text{H}_2\text{O}$ indicating the incomplete transformation of the material into Co_3O_4 . The crystallite sizes of samples were calculated using the Debye-Scherrer equation [40], and all Co_3O_4 materials showed crystallite sizes varying from 5.8 to 17.1 nm, while commercial Co_3O_4 has a much higher crystallite size of 54.6 nm (Table 1). Fig. 1b shows the low angle PXRD patterns for the cobalt oxides calcined at different temperatures. Both Co-250 and Co-350 show PXRD lines in the low angle region indicating the existence of a mesoporous structure, and Co-150, Co-450 as well as commercial Co_3O_4 failed to give diffraction lines in the low angle region indicating the absence of a mesostructure [33]. Mesopores of UCT type materials are formed by connected inter particle voids. Heat treatment increases the average size of nano-size particle

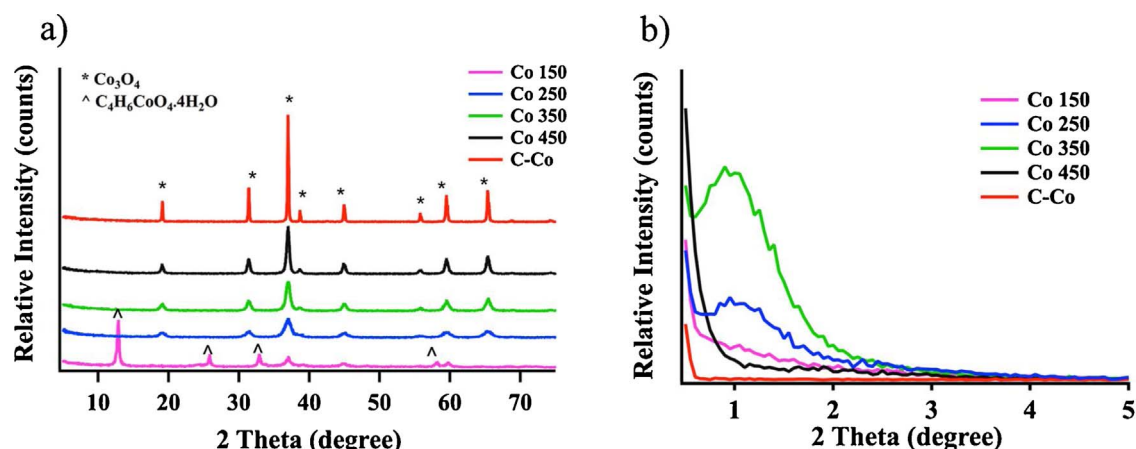


Fig. 1. Powder X-ray diffraction patterns (a) wide angle PXRD (b) low angle PXRD, of Co-X (X = 150, 250, 350, and 450 °C) and commercial Co₃O₄ (C-Co) samples.

Table 1

Structural parameters of mesoporous cobalt oxide materials.

Catalyst	BET surface area (m ² /g)	BJH Des. pore volume (cm ³ /g)	BJH Des. pore diameter (nm)	low angle diffraction position (nm)	crystallite size (nm)
Co-150	6	0.02	b	b	2.5
Co-250	117	0.27	4.7	7.3	5.8
Co-350	73	0.31	8.4	8.7	8.2
Co-450	43	0.27	12.7	b	17.1
C-Co	2	0.01	b	b	63.1

b signifies not applicable.

building blocks due to the unit cell expansion which subsequently increases the size of interparticle voids [33]. Upon heat treatment further condensation of inorganic walls leads to an increase in *d*-spacings and thereby change the unit cell dimensions in inverse micelle-templated mesoporous materials [33]. Unit cell expansion makes the diffraction lines shift towards lower angle (2θ) in the PXRD pattern [41,42]. The low angle peak position of Co-350 shifted to smaller 2θ values compared to Co-250, suggesting Co-350 has much larger particle size compared to Co-250 [38]. The low angle line position correlates well with the calculated average size of the particles (Table 1), which confirms that the heat treatment increases the particle size of UCT Co₃O₄.

3.1.2. N₂ sorption studies

N₂ adsorption-desorption isotherms shown in Fig. 2, a display characteristic Type IV isotherms for Co-250 and Co-350 displaying the mesoporous nature of the material. These results are in good agreement

with the low angle PXRD data where only Co-250 and Co-350 gave low angle peaks. The H1 hysteresis loop exhibits the nature of well ordered uniform pores which give rise to a narrow pore size distribution [43,44]. Furthermore, Co-150 exhibits a non-porous nature having the type II isotherm, that gives the lowest surface area among all other materials. All of them showed monomodal pore size distributions in the BJH pore diameter curves except Co-150 (Fig. 2b). The BJH pore diameter increases with an increase of calcination temperature revealing the unique nature of the soft templated UCT synthesis method where pore expansion is observed upon heat treatment [33]. The highest surface area was obtained for the material calcined at 250 °C, and further heat treatment caused a decrease in surface area. Table 1 summarizes structural features of mesoporous Co₃O₄ synthesized under different conditions.

3.1.3. Scanning electron microscopy/Transmission electron microscopy (SEM/TEM)

FE-SEM images show the morphology of Co-250, 350 and 450 as flower like round particles, which are made out of nano-sized plates (Fig. 3a–b). TEM images (Fig. 3d–f) show a particle size expansion upon heat treatment from 250 to 450 °C which correlates well with PXRD data. HR-TEM images reveal the crystalline nature of the material. As shown in HRTEM, lattice fringes of 0.24 nm can be indexed to the {311} planes of the cubic spinel Co₃O₄ crystal structure.

3.1.4. X-ray photoelectron spectroscopy (XPS)

The Co 2p spectra consist of two peaks which can be assigned to Co 3p_{3/2} and Co 3p_{1/2}, located at binding energies of 780 and 795 eV respectively, which consistent with the presence of spinel Co₃O₄ phase

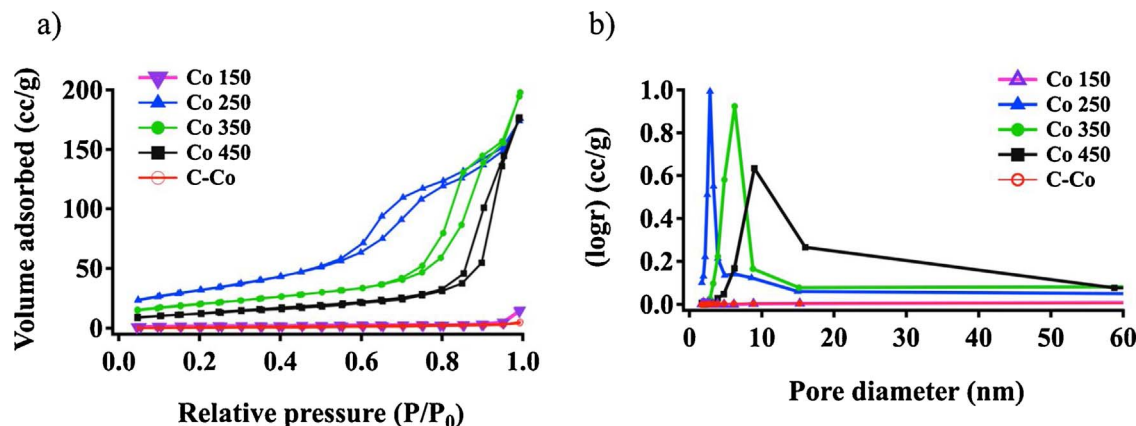


Fig. 2. (a) N₂ sorption isotherms (b) BJH desorption pore size distributions for Co-X (X = 150, 250, 350, and 450).

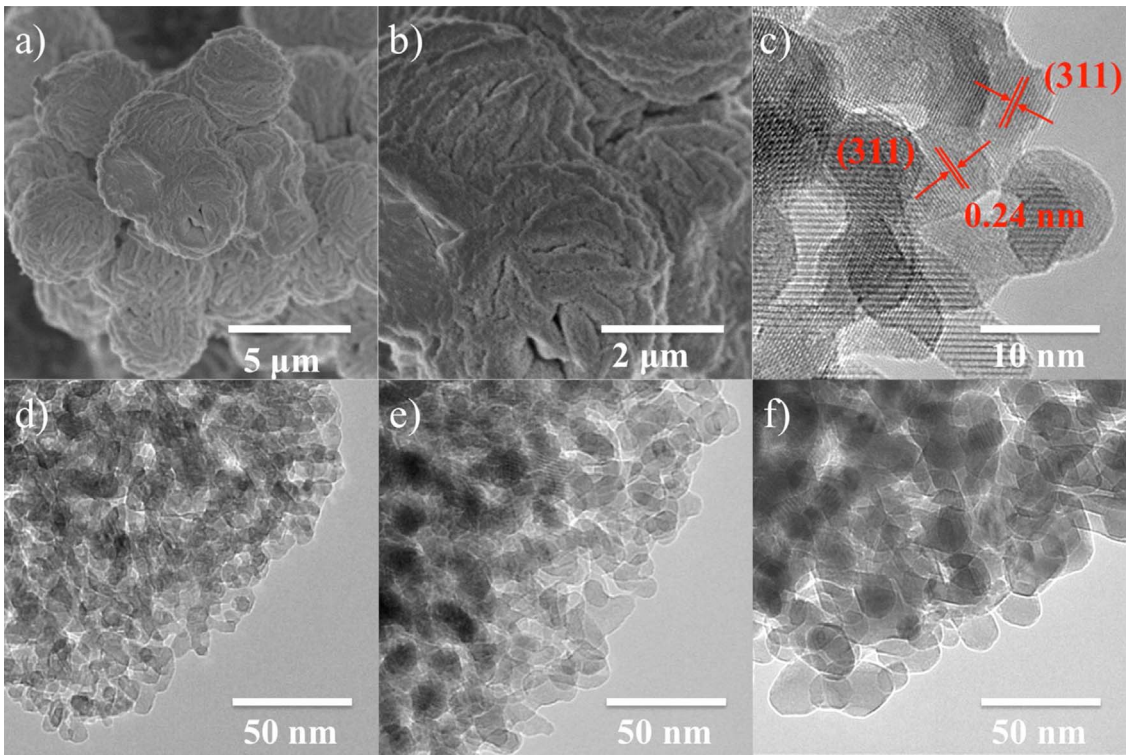


Fig. 3. (a, b) FE-SEM of Co-250, (c) HR-TEM of Co-250, TEM images of (d) Co-250, (e) Co-350 and (f) Co-450 showing the particle size growth with the heat treatment.

(Fig. 4b) [45]. Deconvoluted Co 2p spectra gives peaks around 779 and 795 eV, which are attributed to Co^{3+} , while peaks around 781 and 797 eV are assigned for Co^{2+} [46]. A broad peak for the O 1s spectrum around 526–534 eV suggests the presence of multiple oxygen species in the material (Fig. 4a). The deconvoluted O 1s spectrum gave peaks at 529, 531 and 533 eV binding energies, which can be ascribed to surface lattice oxygen (O_L), surface adsorbed hydroxyl groups (O_OH) and chemisorbed water (O_MW) respectively [38]. Peak area percentages for Co^{3+} , Co^{2+} and different oxygen components are tabulated in Table 2. With heat treatment, the percent Co^{3+} content in the materials increases and Co-250 has the highest $\text{Co}^{2+}/\text{Co}^{3+}$ ratio while having the lowest amount of lattice oxygen.

Table 2
Summary of area percentages of different elemental components, obtained from deconvoluted XPS spectra.

Sample	% Area				
	Co 2p _{3/2}		O 1s		
	Co ²⁺	Co ³⁺	O _{MW}	O _{OH}	O _L
Co-250	28.0	72.0	9.2	30.5	60.3
Co-350	25.2	74.8	10.5	28.1	61.4
Co-450	21.5	78.5	11.2	26.9	61.8

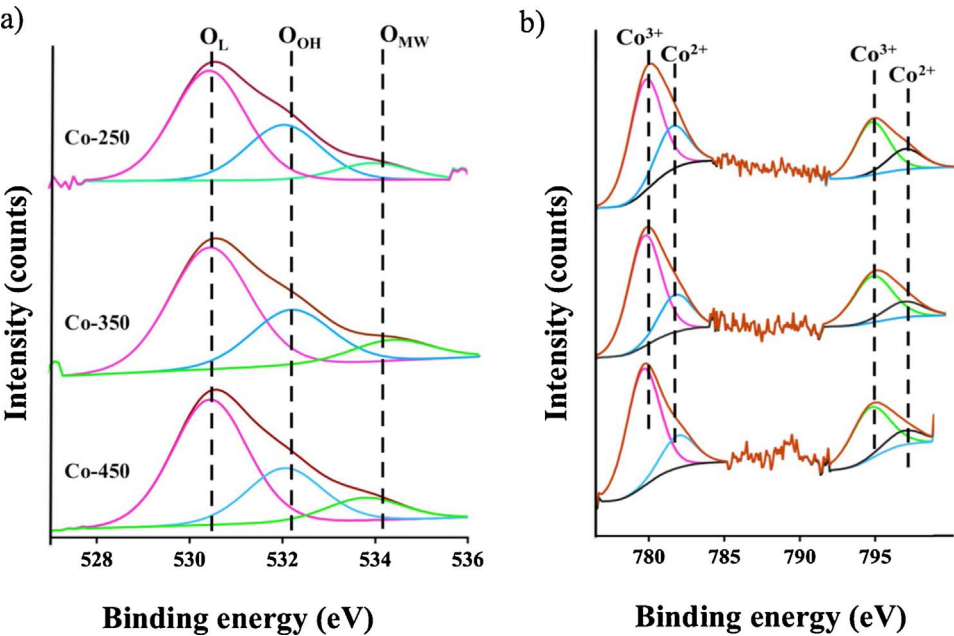


Fig. 4. X-ray photoelectron spectroscopy (XPS) analysis: (a) O 1s and (b) Co 2p deconvoluted XPS spectra of cobalt oxides (Co-X; X = 250, 350 and 450).

3.1.5. Raman spectroscopy

Raman spectral data for mesoporous cobalt oxide materials are displayed in Fig. S2. A clear phase transformation was observed at calcination temperatures between 150 °C to 250 °C, whereas the material transformed to pure Co_3O_4 phase above 250 °C. Raman spectra for Co-250, Co-350, and Co-450 show a similar pattern, however peak intensities increase with heat treatment. Among the vibrational modes of spinel Co_3O_4 , only the A_{1g} , E_g , and F_{2g} modes are Raman active [47]. Peaks around 695, 523 and 477 cm^{-1} are assigned to the A_{1g} , E_g and F_{2g} lattice vibration modes of the spinel structure, respectively [25,48,49]. Yang et al. suggested that the Raman peak observed at 457 cm^{-1} is due to the O–Co–O bending mode of cobalt oxide [50]. Moreover, Nikolov et al. reported the Raman spectrum of $\text{C}_4\text{H}_6\text{CoO}_4\cdot 4\text{H}_2\text{O}$ and they assigned peaks at 1031 and 1059 cm^{-1} for CH_3 rocking vibrations [51]. Bands around 1511 and 3115 cm^{-1} were assigned to CO_2 asymmetric stretching and O–H symmetric stretching modes, respectively [51]. Raman spectra are in good agreement with observed PXRD data and it reflects that the full conversion of the material to cubic crystalline Co_3O_4 happens at temperatures > 250 °C and Co-150 consists of mixed phase cobalt oxide materials.

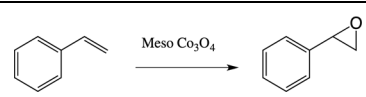
3.1.6. Thermo gravimetric mass spectrometry (TGA-MS)

Fig. S1 shows the TGA-MS curves for as synthesized cobalt oxides subjected to different heating cycles. All cobalt oxides show a minor weight loss (approximately 2%) below 200 °C due to the removal of surface adsorbed water. However, Co-150 (Fig. S1a) shows a significant difference in its thermal stability compared to the remaining cobalt oxides, which were subjected to higher heating cycles. The drastic weight loss occurs from 225 °C up to 400 °C and is due to the emission of CO , CO_2 gases water vapor. Co-150 is a mixed phase containing Co_3O_4 along with $\text{C}_4\text{H}_6\text{CoO}_4\cdot 4\text{H}_2\text{O}$, and is converted to pure Co_3O_4 by emitting CO , CO_2 gases, and H_2O vapor upon heating the material to 225–400 °C [25,38]. Despite the minor weight loss due to the removal of surface adsorbed water, Co-250, Co-350, and Co-450 are stable up to 800 °C. For all the samples above the calcination temperature > 250 °C, a major weight loss at 800 °C was observed, which can be correlated with the removal of lattice oxygen of the material [25].

3.2. Optimization of reaction conditions

Catalytic epoxidation reactions of alkenes with heterogeneous [14] and homogeneous [10,52] systems have been discussed extensively in the literature. In this work styrene was initially selected as the screening molecule to understand and to optimize the reaction conditions. Atmospheric air was bubbled at a rate of 10 mL/min in all cases unless otherwise noted. In order to find out the best catalyst, Co_3O_4 calcined at different temperatures were tested (Table 3). Commercial

Table 3
Catalyst selection in epoxidation of styrene.^a

				
Entry	Catalyst	Conversion ^b (%)	Selectivity ^c (%)	TOF ^d
1	Co-150	20	80	4.8
2	Co-250	89	93	21.1
3	Co-350	46	91	11.1
4	Co-450	32	66	7.7
5	C- Co_3O_4	30	87	7.2

^a Reaction conditions: styrene (3 mmol), catalyst (10 mg), DMF (5 mL), airflow 10 mL/min, 100 °C, 3 h.

^b Conversions were determined by GC–MS based on the concentration of styrene.

^c The other product was benzaldehyde.

^d TOF = no of moles of styrene converted per mole of catalyst/reaction time (h).

Co_3O_4 exhibited lower reactivity but higher than Co-150. This could be justified, since Co-150 is not fully converted to crystalline Co_3O_4 and contains $\text{C}_4\text{H}_6\text{CoO}_4\cdot 4\text{H}_2\text{O}$ that might not be as active as the cubic phase of Co_3O_4 for the desired reaction. A remarkable effect of the catalyst's surface area on the catalytic activity was encountered. However, Co150 could be excluded from the trend with respect to surface area because some of the Co in this sample stays in the form of $\text{C}_4\text{H}_6\text{CoO}_4\cdot 4\text{H}_2\text{O}$ and introduces Co^{2+} to the system, which can perform homogeneous chemistry [53,54]. Co-250, which has the highest surface area, showed the best performance over the others, and therefore was selected to use for further optimization. Using Co-250 as the catalyst and maintaining all other reaction conditions constant, solvents with different polarities were tested (entry 1–3, Table 4). The same temperature (100 °C) was applied in all cases (unless otherwise noted) to avoid the effect of temperature. Among the tested solvents, dimethylformamide (DMF) gave the highest conversion (> 99%) with a selectivity of 93% (entry 2, Table 4). The solvent free system gave an epoxide conversion of 35% within four hours, though the selectivity is low (43%), due to the formation of benzaldehyde as the byproduct (entry 7, Table 4). This signifies that the catalytic system could exhibit a decent activity even without the assistance of any solvent system. Nevertheless, the combination of the catalyst solvent system enhances the overall performance in the reaction. Catalyst loading is another factor, which has to be considered especially in these types of organic reactions, because in large scale synthesis and industrial processes, higher turnover numbers are required. Increasing the catalyst amount from 10 to 50 mg did not have a significant effect on the turnover number (entry 5, Table 4), revealing that a low catalyst loading of 10 mg is sufficient to drive the reaction. A control experiment was done without any catalyst, which gave rather low conversion of 12% (entry 9, Table 4). To investigate the effect of sacrificial oxidant, aqueous TBHP was added to the system. The conversion was almost similar to the one without TBHP, but gave a lower selectivity (86%) (entry 8, Table 4). Notably no conversion was detected when the reaction was done under N_2 atmosphere, which indicates that air is the oxidant in this case (entry 6, Table 4). Therefore, the Co-250 catalyst and DMF as the solvent with a 10 mg catalyst loading were selected as optimized conditions and used for further experiments, if not otherwise specified.

3.3. Substrate scope

In order to establish the broad applicability of this approach, several alkenes were subjected to the epoxidation reaction. Different types of aliphatic, aromatic, cyclic and alkenes with different functional groups were selected while using the optimized reaction conditions. The meso Co-250 catalyst was found to be effective in epoxidation of a wide range of aromatic, aliphatic, primary, secondary, and cyclic alkenes (entry 1–11, Table 5). In the case of relatively bulky alkenes such as *cis*-stilbene, a high conversion (87%) and excellent selectivity (96%) was achieved, though the reaction time required was comparatively high (24 h) (entry 7, Table 5). Cyclic alkenes also gave very high conversion and selectivity (> 78%) (entry 6, 8, 10–11, Table 5). Epoxidation of ethynyl cyclohexene gave 100% selectivity with high yield (91%) implying superior chemoselectivity of the catalyst towards selective oxidation of double bonds in the presence of reactive alkyne groups (entry 6, Table 5). The effect of electron donating and withdrawing substituents on the epoxidation, was further analyzed using substituted styrene compounds. α methyl substituted styrene required much higher reaction time (12 h) to give > 99% conversion (entry 2, Table 5). However, para substituted styrenes were less affected compared to α substituents (entry 3–5, Table 5). Alkenes with different functional groups (hydroxyl, alkyne) were also examined and found to give decent conversion and selectivity (entry 6, 9–10, Table 5). Results showed that the presence of electron donating and withdrawing groups in the para position has a significant effect on the reaction rate. Methyl and methoxy substituents exhibited much lower rates whereas the chloro

Table 4
Optimization of the reaction conditions.^a

Entry	Solvent	Temp. (°C)	Time (h)	Oxidant	Conversion ^b (%)	Selectivity ^c (%)	TOF ^d
1	Toluene	100	4	Air	3	16	0.5
2	DMF	100	4	Air	> 99	93	17.9
3	ACN	80	4	Air	1	25	0.2
4 ^e	Toluene	100	4	Air	9	25	1.6
4	DMF	100	3	Air	89	93	21.4
5 ^f	DMF	100	3	Air	87	92	21.0
6 ^g	DMF	100	4	N ₂	0	N/A	N/A
7 ^h	None	100	4	Air	35	43	6.3
8 ⁱ	DMF	100	4	Air	> 99	86	17.9
9 ^j	DMF	100	4	Air	11	91	1.9

^a Reaction conditions: styrene (3 mmol), catalyst Co-250 (10 mg), solvent (5 mL), airflow 10 mL/min, 100 °C.

^b Conversions were determined by GC–MS based on the concentration of styrene.

^c The other product was benzaldehyde.

^d TOF = no of moles of styrene converted per mole of catalyst/reaction time (h).

^e 1 mL of toluene.

^f 50 mg catalyst.

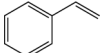
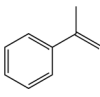
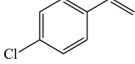
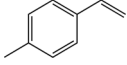
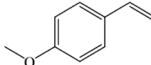
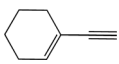
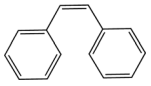

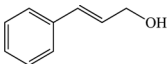
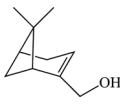

^g N₂ balloon.

^h Solvent free (10 mmol styrene).

ⁱ With 3 mmol aq. TBHP.

^j No catalyst.

Table 5
Aerobic oxidation of alkenes to epoxides by meso Co-250.^a

Entry	Substrate	Time (h)	Conversion ^b (%)	Selectivity ^c (%)	TOF ^d
1		4	> 99	93	17.9
2		12	> 99	64	6.0
3		3	93	93	22.4
4		4	83	90	15.0
5		4	23	50	4.2
6		24	91	100	2.7
7		24	87	96	2.6
8		4	65	86	11.8
9		48	31	26	0.5
10		4	40	88	7.2
11		3	87	78	21.0

^a Reaction conditions: alkene (3 mmol), Co-250 (10 mg), DMF (5 mL), 100 °C, airflow 10 mL/min.

^b Conversion and selectivity was determined by GC–MS based on the concentration of alkene.

^c The other product was corresponding aldehyde.

^d TOF = no of moles of alkene converted per mole of catalyst/reaction time (h).

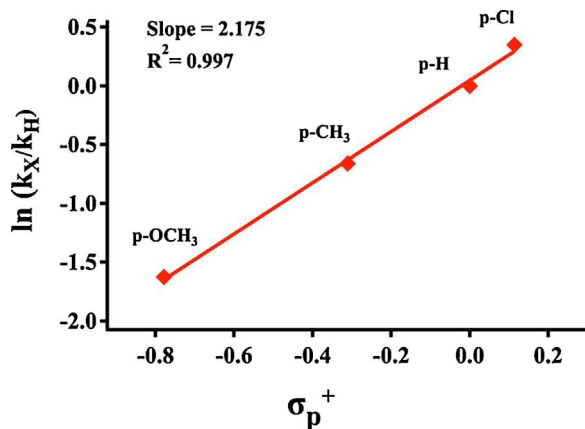


Fig. 5. Hammett plot of competitive epoxidation of para-substituted styrenes. Reaction conditions: styrene (3 mmol), catalyst (10 mg), solvent (5 mL), 100 °C, air flow (10 mL/min), time (90 min). A linear relationship between $\ln(k_X/k_H)$ and the Brown-Okamoto constant (σ_p^+) for para-substituted styrenes was obtained with a slope (ρ) of 2.175, which indicated the formation of a negatively charged intermediate. k_X and k_H are rate constants for substituted and unsubstituted styrene, respectively.

substituent gave higher rates compared to unsubstituted styrene (entry 3–5, Table 5). Electronic or steric effects of the aromatic substituent groups on the reaction rate could be explained using the Hammett equation [55–57]. Relative rates of epoxidation of p-OCH₃, p-CH₃, p-H and p-Cl substituted styrenes were calculated and a linear relationship was observed for the plot of $\ln(k_X/k_H)$ vs the Brown-Okamoto constant (σ_p^+) (Fig. 5). The reaction constant (ρ) which is the slope of the graph (2.175) suggests the formation of a negatively charged transition state in the rate determining step of the styrene epoxidation reaction [55].

3.4. Reusability and heterogeneity

The reusability of the catalyst was examined by repeating the reaction several times using the same catalyst. Styrene epoxidation was used as the model reaction. At the end of the reaction, the catalyst was separated by filtration, washed several times with DMF and then with ethanol, and heated in the oven at 250 °C for one hour. Heating could remove the adsorbed species and reactivate the catalyst by opening pores. Even after four reaction cycles, the activity remained almost unchanged indicating the high reusable capacity of the catalyst (Fig. 6a). Observations were confirmed by comparing the PXRD patterns of the catalyst before and after reuse (Fig. 6b). No difference between PXRD patterns was noted implying that the crystal structure

was still preserved for the used catalyst. Heterogeneity of the material was confirmed by analyzing the reaction filtrate by ICP-MS, which gave minute amounts of cobalt species (3 ppm) in the solution after the reaction.

3.5. Kinetic and mechanistic study

Depending on the catalytic activity and the reported data, mechanistic details of the reaction were investigated. Radical scavenger molecules, 2,6-di-tert-butyl-4-methylphenol and sodium pyruvate, were used to check if any radical species are involved in the reaction. Introduction of radical scavengers had a significant effect on the reaction progress. Use of scavengers totally diminished the reaction and no epoxide products were detected. These results suggest that a radical intermediate is involved in the reaction pathway and the observations are consistent with reported literature [20]. In order to study the effect of peroxides on the reaction rate, *tert*-butyl hydroperoxide (TBHP) was used as a radical initiator. Addition of TBHP showed the conversion to be the same as when the reaction was performed without any peroxides. Nevertheless, the selectivity towards the epoxide was poor (86%), due to the formation of unwanted side products, benzaldehyde and benzoic acid. For the rate and kinetic energy calculations, continuous sampling was done in half an hour intervals and the conversions were determined with GC-MS. Kinetic studies for epoxidation reaction with the Co-250 at 100 °C, exhibit first order kinetics with respect to the styrene with a rate constant of 0.015 min⁻¹ (Fig. S3). Activation energy was calculated using the Arrhenius equation [58] and gave a value of 8.7 kcal/mol (Fig. S4).

4. Discussion

In this study mesoporous Co₃O₄ was synthesized by evaporation induced self-assembly method and employed as an efficient catalyst for liquid phase aerobic alkene epoxidation. Epoxidation reactions were carried out with excellent yield and selectivity, most importantly under aerobic conditions, eliminating the use of sacrificial oxidizing agents. Epoxidation without an external oxidizing agent is a challenge as in most cases peroxide reagents have been utilized [10,13,16]. Among the mesoporous Co₃O₄ materials calcined at different temperatures, Co-250 was found to be the most active and Co-450 is the least. This trend of reactivity strongly correlates with the surface area of the material, where Co-250 exhibits the highest surface area and the surface area decreases as Co-250 > Co-350 > Co-450. Higher surface area leads to weakening of the Co-O bond and exposure of more active sites on the surface, thereby facilitating these oxidation reactions [26,59]. In

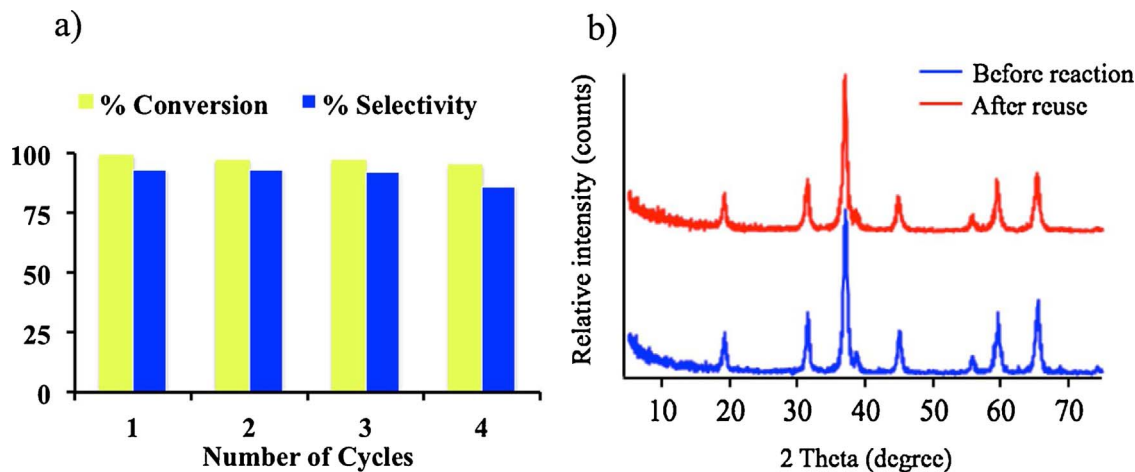


Fig. 6. a) Reusability test of the catalyst. b) PXRD of Co-250 before and after the reaction; without noticeable change in the diffraction pattern. Reaction condition: styrene (3 mmol), Co-250 (10 mg), DMF (5 mL), 100 °C, airflow 10 mL/min. Conversion and selectivity were determined with GC-MS based on the concentration of styrene.

addition, mesoporosity of the material also plays a significant role by reducing mass transfer limitations of the material, thereby facilitating the adsorption and diffusion of the substrate over the catalyst surface [31]. This is in good agreement with observed lower activity of commercial nonporous Co_3O_4 (30% conversion) compared to mesoporous Co-250 (93% conversion). According to the literature, surface defects of the Co_3O_4 enhance the catalytic activity of the material towards the oxidation reactions [38,60]. Fei et al. reported Co_3O_4 nanotubes with higher oxygen vacancies on the surface, giving excellent activity in catalytic combustion of methane [60]. Moreover, surface hydroxyl groups are associated with the Brönsted acidity of metal oxides [61]. An increase in Brönsted acidity of cobalt oxide catalysts is reported to have higher catalytic activity towards epoxidation reactions [17,62]. As revealed by XPS data (Table 2), Co-250 exhibited the highest percent of oxygen vacancies and surface hydroxyl groups, implying that Co-250 has the highest surface defects among all materials studied [63]. This clearly signifies that along with surface area, surface defects also play an important role in terms of catalytic activity. The effect of solvent was identified through a solvent screening test and DMF was shown to be the most effective solvent. More polar solvents, especially those that contain carboxylic groups were found to be more effective in epoxidation reactions [20,64]. It has been reported that DMF has a high capacity to dissolve molecular oxygen, which then can be converted into active oxygen species [20]. Moreover, DMF plays a major role in the mechanism of epoxidation by changing the coordination environment of Co^{2+} which changes from octahedral where these tetrahedral sites act as true active sites for the desired reaction [65]. Decrease of the solvent volume increases the number of collisions per unit time, consequently showed slight increase in the conversion even though the selectivity is low (entry 4, Table 4). Epoxidation of various types of alkenes including aromatic, aliphatic, cyclic, and long chain alkenes was carried out successfully in this current study with high turnover numbers. Longer reaction times are required for the alkenes containing bulky groups. This may be due to the steric hindrance of the double bond, which block the coordination between double bond and the metal center. When there are other functional groups present along with the double bond, the chemoselectivity of the current protocol is quite notable. 1-ethynyl cyclohexene (entry 6, Table 5) gives the corresponding epoxide with 100% selectivity without affecting the triple bond, although triple bond can be oxidized in the presence of other catalysts [66–68]. However, poor selectivity towards epoxide was observed in alkenes, which contain a hydroxyl group. Cinnamyl alcohol (entry 9, Table 5) gives 23% of corresponding epoxide and gives cinnamaldehyde as the major product. Extended conjugated systems generally have lower overall energy and therefore high stability [69]. Thus cinnamyl alcohol prefers to retain the extended conjugation by converting into cinnamaldehyde, rather than giving the epoxide where conjugation is absent. However, (–)-myrtenol (entry 10, Table 5) was able to give epoxide with 88% selectivity, while keeping the hydroxyl group intact. 1,5-cyclooctadiene, which has two double bonds in the same molecule, gave one double bond oxidized product with significant selectivity (86%) (entry 8, Table 5). Overall the catalytic system was able to give decent conversion and selectivity for a wide range of double bond containing systems.

The proposed mechanism for the reaction, depending on reported literature and observed data is presented in the schematic diagram S1. DMF molecules will first coordinate to the cobalt cations present in Co_3O_4 , through oxygen atoms of DMF giving a $\text{Co(II)}\text{--DMF}$ complex [20]. This complex further coordinates with molecular oxygen to form a $\text{DMF--Co(III)OO}\cdot$ superoxo type complex which facilitates the addition of oxygen to the double bond of the alkene [20]. Tang et al. reported the tetrahedrally coordinated Co^{2+} sites together with DMF ligands play a significant role in the activation of O_2 for the epoxidation reaction [65]. Coordination environment of Co^{2+} changes from octahedral to tetrahedral due to the DMF treatment and these tetrahedral Co^{2+} complexes form true active sites for the epoxidation reaction

[65]. The alkene-superoxo complex then undergoes migratory insertion to form cobalt peroxo complex (I), followed by formation of the four membered cyclic radical intermediate (II) [17,20]. Pruß et al. reported ligand field strength is a major factor to decide where the bond cleavage occurs in the peroxo complex, which determines the selectivity for each product [70]. We believe DMF acts as a ligand to drive the reaction in the direction which gives high selectivity for epoxide as compared to DMF free conditions [71]. Due to the metal-DMF complex formation, the delocalization of the C=O electron cloud would decrease its double bond character and therefore a red shift and a lower intensity peak could be observed in the Infrared (IR) spectrum [72]. We did IR analysis for fresh catalyst, using catalyst and pure DMF (Fig. S5). In the used catalyst, apart from the peaks for cobalt ions there are additional peaks appear around 1675, 1380, and 1250 cm^{-1} with lower intensity compared to peaks in pure DMF, suggesting the complex formation between cobalt and DMF [73]. The IR peak at 1675 cm^{-1} , which is due to C=O stretching vibrations has lower intensity and has a red shift for the used catalyst compared to that of DMF. As the final step of the catalytic cycle, the radical intermediate reacts with another styrene molecule to give the epoxide. Decomposition of the cyclic radical yields the corresponding aldehyde. Breakdown of complex (I) releases Co^{2+} , which is oxidized back to Co^{3+} by molecular O_2 to regenerate the catalyst. The PXRD pattern after the reaction was similar to the original structure, which verifies regeneration of the catalyst. Addition of a radical inhibitor terminated the reaction, confirming the reaction pathway consists of radical intermediates. Sebastian et al. reported that stabilization of cyclic intermediate (I), would lead to higher reaction rates [20]. In this context, if a negatively charged intermediate forms, introduction of electron withdrawing groups to the para position should increase the reaction rate and vice versa [36]. We encountered a significant decrease in reaction rate, when an electron donating group was introduced to the para position of styrene and a higher rate for electron withdrawing groups. Formation of a negatively charged transition state at the rate determining step was further confirmed by the Hammett plot, which gave a positive slope of 2.175. A continuous supply of air is crucial in this reaction, as the consumed oxygen has to be replaced by oxygen from air. When the reaction is done under a nitrogen environment, no conversion was detected.

Temperature has been found to have a significant effect in the reaction rate. The kinetic studies revealed that the reaction follows first order kinetics and it is also consistent with reported literature on styrene epoxidation [74,75]. The calculated activation energy (8.7 kcal/mol) is in good agreement with reported values in the literature for homogenous and heterogeneous systems [4,75]. Yadav et al. [4] reported an activation energy of 7.26 kcal/mol for heteropolyacids and a phase transfer catalyst system and Liang et al. [75] reported 100.4 kcal/mol for a Prussian blue analogue catalytic system. However, in both of these cases a peroxide reagent was utilized as the oxidizing agent. Therefore our low energy reaction pathway for alkene epoxidation, even without the presence of sacrificial peroxide agents, could be attributed to the superior catalytic activity of mesoporous UCT Co_3O_4 material.

5. Conclusion

In summary, we have reported that mesoporous cobalt oxide acts as an efficient catalyst for catalytic epoxidation of alkenes. Cobalt oxides with varied surface areas, pore sizes, and pore diameters were synthesized by adjusting the calcination temperature during the synthesis route. The optimized catalyst was able to oxidize a diverse range of alkenes including aromatic, aliphatic, long chain, and cyclic alkenes with excellent conversion and selectivity. Mechanistic studies revealed that the reaction follows first order kinetics and the formation of a negatively charged transition state in the rate-determining step. High surface area, mesoporosity, and surface oxygen vacancies were identified as the major contributors to the catalytic activity. Hence Co-250

was found to be the most active material. Avoiding the use of sacrificial oxidizing agents such as peroxides and use of the “greenest” oxidant air is highly significant in this study in terms of performing green and environmentally benign catalysis. The catalysts could be recycled and reused up to four catalytic cycles without significant loss of activity. Our catalytic protocol can serve as a benchmark in terms of designing economical and ecofriendly catalysts for peroxide free alkene epoxidation reactions.

Notes

The authors declare no competing financial interest.

Acknowledgements

We thank the Chemical, Geochemical and Biosciences Division of the Office of Basic Energy Sciences, Office of Science, U.S. Department of Energy for supporting this work under grant DE-FG02-86ER13622-A000.

Appendix A. Supplementary data

Supplementary data associated with this article can be found, in the online version, at <http://dx.doi.org/10.1016/j.apcatb.2017.09.053>.

References

- [1] K. Ebitani, Creation of a monomeric Ru species on the surface of hydroxyapatite as an efficient heterogeneous cat for aerobic alcohol oxidation, *J. Am. Chem. Soc.* 2000 (2000) 7144.
- [2] S. Biswas, A.S. Poyraz, Y. Meng, C. Kuo, C. Guild, H. Tripp, S.L. Suib, Ion induced promotion of activity enhancement of mesoporous manganese oxides for aerobic oxidation reactions, *Appl. Catal. B Environ.* 165 (2015) 731–741, <http://dx.doi.org/10.1016/j.apcatb.2014.10.055>.
- [3] J.S. Jirkovský, M. Busch, E. Ahlberg, I. Panas, P. Krtil, Switching on the electro-catalytic ethene epoxidation on nanocrystalline RuO₂, *J. Am. Chem. Soc.* 133 (2011) 5882–5892, <http://dx.doi.org/10.1021/ja109955w>.
- [4] G.D. Yadav, A.A. Pujari, Epoxidation of styrene to styrene oxide: synergism of heteropoly acid and phase-transfer catalyst under Ishii-Venturello mechanism, *Org. Process Res. Dev.* 4 (2000) 88–93, <http://dx.doi.org/10.1021/op990055p>.
- [5] R. Neumann, M. Dahan, A ruthenium-substituted polyoxometalate as an inorganic dioxygenase for activation of molecular oxygen, *Nature* 388 (1997) 353–355, <http://dx.doi.org/10.1038/41039>.
- [6] N.S. Patil, R. Jha, B.S. Uphade, S.K. Bhargava, V.R. Choudhary, Epoxidation of styrene by anhydrous t-butyl hydroperoxide over gold supported on Al₂O₃, Ga₂O₃, In₂O₃ and Ti₂O₃, *Appl. Catal. A Gen.* 275 (2004) 87–93, <http://dx.doi.org/10.1016/j.apcata.2004.07.023>.
- [7] I. Fehete, Y. Wang, J.C. Védrine, The past, present and future of heterogeneous catalysis, *Catal. Today* 189 (2012) 2–27, <http://dx.doi.org/10.1016/j.cattod.2012.04.003>.
- [8] B.S. Lane, K. Burgess, Metal-catalyzed epoxidations of alkenes with hydrogen peroxide, *Chem. Rev.* 103 (2003) 2457–2473, <http://dx.doi.org/10.1021/cr020471z>.
- [9] D.S. Pinnaduwa, L. Zhou, W. Gao, C.M. Friend, Chlorine promotion of styrene epoxidation on Au(111), *J. Am. Chem. Soc.* 129 (2007) 1872–1873, <http://dx.doi.org/10.1021/ja068245k>.
- [10] C. Wang, H. Yamamoto, Tungsten-catalyzed asymmetric epoxidation of allylic and homoallylic alcohols with hydrogen peroxide, *J. Am. Chem. Soc.* 136 (2014) 1222–1225, <http://dx.doi.org/10.1021/ja111379e>.
- [11] A. Bhaumik, T. Tatsumi, Organically modified titanium-rich Ti-MCM-41, efficient catalysts for epoxidation reactions, *J. Catal.* 189 (2000) 31–39, <http://dx.doi.org/10.1006/jcat.1999.2690>.
- [12] Y. Jin, D. Zhuang, N. Yu, H. Zhao, Y. Ding, L. Qin, J. Liu, D. Yin, H. Qiu, Z. Fu, D. Yin, Epoxidation of styrene over gold nanoparticles supported on organic-inorganic hybrid mesoporous silicas with aqueous hydrogen peroxide, *Microporous Mesoporous Mater.* 126 (2009) 159–165, <http://dx.doi.org/10.1016/j.micromeso.2009.05.032>.
- [13] Y. Jin, P. Wang, D. Yin, J. Liu, H. Qiu, N. Yu, Gold nanoparticles stabilized in a novel periodic mesoporous organosilica of SBA-15 for styrene epoxidation, *Microporous Mesoporous Mater.* 111 (2008) 569–576, <http://dx.doi.org/10.1016/j.micromeso.2007.08.036>.
- [14] K. Kamata, K. Yonehara, Y. Sumida, K. Hirata, S. Nojima, N. Mizuno, Efficient heterogeneous epoxidation of alkenes by a supported tungsten oxide catalyst, *Angew. Chem. Int. Ed. Engl.* 50 (2011) 12062–12066, <http://dx.doi.org/10.1002/anie.201106064>.
- [15] R. Anand, S.S. Shevade, R.K. Ahedi, S.P. Mirajkar, B.S. Rao, Epoxidation of styrene with TBHP/O₂ over ferrierite (FER) type molecular sieves, *J. Catal.* 62 (1999) 209–213.
- [16] W. Jia, Y. Liu, P. Hu, R. Yu, Y. Wang, L. Ma, D. Wang, Y. Li, Ultrathin CuO nanorods: controllable synthesis and superior catalytic properties in styrene epoxidation, *Chem. Commun.* 51 (2015) 8817–8820, <http://dx.doi.org/10.1039/C5CC02480C>.
- [17] S. Rahman, C. Santra, R. Kumar, J. Bahadur, A. Sultana, R. Schweins, D. Sen, S. Maity, S. Mazumdar, B. Chowdhury, Highly active Ga promoted Co-HMS-X catalyst towards styrene epoxidation reaction using molecular O₂, *Appl. Catal. A Gen.* 482 (2014) 61–68, <http://dx.doi.org/10.1016/j.apcata.2014.05.024>.
- [18] C.V. Rode, U.N. Nehete, M.K. Dongare, Alkali promoted selective epoxidation of styrene to styrene oxide using TS-1 catalyst, *Catal. Commun.* 4 (2003) 365–369, [http://dx.doi.org/10.1016/S1566-7367\(03\)00088-8](http://dx.doi.org/10.1016/S1566-7367(03)00088-8).
- [19] I. Kirm, F. Medina, X. Rodríguez, Y. Cesteros, P. Salagre, J. Sueiras, Epoxidation of styrene with hydrogen peroxide using hydrotalcites as heterogeneous catalysts, *Appl. Catal. A Gen.* 272 (2004) 175–185, <http://dx.doi.org/10.1016/j.apcata.2004.05.039>.
- [20] J. Sebastian, K.M. Jinka, R.V. Jasra, Effect of alkali and alkaline earth metal ions on the catalytic epoxidation of styrene with molecular oxygen using cobalt(II)-exchanged zeolite X, *J. Catal.* 244 (2006) 208–218, <http://dx.doi.org/10.1016/j.jcat.2006.09.005>.
- [21] J. Sun, Q. Kan, Z. Li, G. Yu, H. Liu, X. Yang, Q. Huo, J. Guan, Different transition metal (Fe²⁺, Co²⁺, Ni²⁺, Cu²⁺ or VO²⁺) Schiff complexes immobilized onto three-dimensional mesoporous silica KIT-6 for the epoxidation of styrene, *RSC Adv.* 4 (2014) 2310–2317, <http://dx.doi.org/10.1039/C3RA45599H>.
- [22] B. Tang, X.-H. Lu, D. Zhou, J. Lei, Z.-H. Niu, J. Fan, Q.-H. Xia, Highly efficient epoxidation of styrene and α-pinene with air over Co₂+exchanged ZSM-5 and beta zeolites, *Catal. Commun.* 21 (2012) 68–71, <http://dx.doi.org/10.1016/j.jcatcom.2012.01.029>.
- [23] S.C. Petitto, E.M. Marsh, G.A. Carson, M.A. Langell, Cobalt oxide surface chemistry: the interaction of CoO(100), Co₃O₄(110) and Co₃O₄(111) with oxygen and water, *J. Mol. Catal. A Chem.* 281 (2008) 49–58, <http://dx.doi.org/10.1016/j.molcata.2007.08.023>.
- [24] J. Chen, X. Wu, A. Selloni, Electronic structure and bonding properties of cobalt oxide in the spinel structure, *Phys. Rev. B* 83 (2011) 245204, <http://dx.doi.org/10.1103/PhysRevB.83.245204>.
- [25] C.W. Tang, C. Bin Wang, S.H. Chien, Characterization of cobalt oxides studied by FT-IR, Raman, TPR and TG-MS, *Thermochim. Acta* 473 (2008) 68–73, <http://dx.doi.org/10.1016/j.tca.2008.04.015>.
- [26] C.W. Tang, W.Y. Yu, C.J. Lin, C. Bin Wang, S.H. Chien, Phase transformation in CeO₂-Co₃O₄ binary oxide under reduction and calcination pretreatments, *Catal. Lett.* 116 (2007) 161–166, <http://dx.doi.org/10.1007/s10562-007-9105-x>.
- [27] A. Tuel, S. Gontier, R. Teissier, Zirconium containing mesoporous silicas: new catalysts for oxidation reactions in the liquid phase, *Chem. Commun.* 143 (1996) 651, <http://dx.doi.org/10.1039/cc9960000651>.
- [28] A. Taguchi, F. Schüth, Ordered mesoporous materials in catalysis, *Microporous Mesoporous Mater.* 77 (2005) 1–45, <http://dx.doi.org/10.1016/j.micromeso.2004.06.030>.
- [29] M. Sui, J. Liu, L. Sheng, Mesoporous material supported manganese oxides (MnOx/MCM-41) catalytic ozonation of nitrobenzene in water, *Appl. Catal. B Environ.* 106 (2011) 195–203, <http://dx.doi.org/10.1016/j.apcatb.2011.05.025>.
- [30] A. Tuel, L.G. Hubert-Pfalzgraf, Nanometric monodispersed titanium oxide particles on mesoporous silica: synthesis, characterization, and catalytic activity in oxidation reactions in the liquid phase, *J. Catal.* 217 (2003) 343–353, [http://dx.doi.org/10.1016/S0021-9517\(03\)00078-2](http://dx.doi.org/10.1016/S0021-9517(03)00078-2).
- [31] N.D. Wasalathanthri, A.S. Poyraz, S. Biswas, Y. Meng, C.H. Kuo, D.A. Kriz, S.L. Suib, High-performance catalytic CH₄ oxidation at low temperatures: inverse micelle synthesis of amorphous mesoporous manganese oxides and mild transformation to K₂xMn₈O₁₆ and e-MnO₂, *J. Phys. Chem. C* 119 (2015) 1473–1482, <http://dx.doi.org/10.1021/jp5108558>.
- [32] A.H. Janssen, A.J. Koster, K.P. De Jong, Three-dimensional transmission electron microscopic observations of mesopores in dealuminated zeolite Y, *Angew. Chem. Int. Ed. Engl.* 40 (2001) 1102–1104, [http://dx.doi.org/10.1002/1521-3773\(20010316\)40:6<1102::AID-ANGE11020>3.0.CO;2-6](http://dx.doi.org/10.1002/1521-3773(20010316)40:6<1102::AID-ANGE11020>3.0.CO;2-6).
- [33] A.S. Poyraz, C.-H. Kuo, S. Biswas, C.K. King'andu, S.L. Suib, A general approach to crystalline and monomodal pore size mesoporous materials, *Nat. Commun.* 4 (2013) 2952, <http://dx.doi.org/10.1038/ncomms3952>.
- [34] A.S. Poyraz, W.A. Hines, C.-H. Kuo, N. Li, D.M. Perry, S.L. Suib, Mesoporous Co₃O₄ nanostructured material synthesized by one-step soft-templating: a magnetic study, *J. Appl. Phys.* 115 (2014) 114309, <http://dx.doi.org/10.1063/1.4868680>.
- [35] A.S. Poyraz, C.-H. Kuo, E. Kim, Y. Meng, M.S. Seraji, S.L. Suib, Tungsten-promoted mesoporous group 4 (Ti, Zr, and Hf) transition-Metal oxides for room-temperature solvent-free acetalization and ketalization reactions, *Chem. Mater.* 26 (2014) 2803–2813, <http://dx.doi.org/10.1021/cm501216c>.
- [36] S. Biswas, B. Dutta, K. Mullick, C.-H. Kuo, A.S. Poyraz, S.L. Suib, Aerobic oxidation of amines to imines by cesium-promoted mesoporous manganese oxides, *ACS Catal.* 5 (2015) 4394–4403, <http://dx.doi.org/10.1021/acscatal.5b00325>.
- [37] B. Dutta, S. Biswas, V. Sharma, N.O. Savage, S.P. Alpay, S.L. Suib, Mesoporous manganese oxide catalyzed aerobic oxidative coupling of anilines to aromatic Azo compounds, *Angew. Chem. Int. Ed.* 55 (2016) 2171–2175, <http://dx.doi.org/10.1002/anie.201508223>.
- [38] W. Song, A.S. Poyraz, Y. Meng, Z. Ren, S.Y. Chen, S.L. Suib, Mesoporous Co₃O₄ with controlled porosity: inverse micelle synthesis and high-performance catalytic Co oxidation at –60 °C, *Chem. Mater.* 26 (2014) 4629–4639, <http://dx.doi.org/10.1021/cm502106v>.
- [39] L.R. Pahalagedara, A.S. Poyraz, W. Song, C.-H. Kuo, M.N. Pahalagedara, Y.-T. Meng, S.L. Suib, Low temperature desulfurization of h₂ S: high sorption capacities by mesoporous cobalt oxide via increased H₂ S diffusion, *Chem. Mater.* 26 (2014) 6613–6621, <http://dx.doi.org/10.1021/cm503405a>.

- [40] L. Alexander, H.P. Klug, Determination of crystallite size with the x-ray spectrometer, *J. Appl. Phys.* 21 (1950) 137–142, <http://dx.doi.org/10.1063/1.1699612>.
- [41] M. Zokaie, D.S. Wragg, A. Grønvald, T. Fuglerud, J.H. Cavka, K.P. Lillerud, O. Swang, Unit cell expansion upon coke formation in a SAPO-34 catalyst: a combined experimental and computational study, *Microporous Mesoporous Mater.* 165 (2013) 1–5, <http://dx.doi.org/10.1016/j.micromeso.2012.07.054>.
- [42] M.A. Rodriguez, J.F. Browning, C.S. Frazer, C.S. Snow, R.G. Tisost, E.P. Boespflug, Unit cell expansion in ErT₂ films, *Powder Diff.* 22 (2007) 118–121, <http://dx.doi.org/10.1154/1.2737462>.
- [43] K.S.W. Sing, D.H. Everett, R.A.W. Haul, L. Moscou, R.A. Pierotti, J. Rouquérol, T. Siemieniowska, Reporting physisorption data for gas/solid systems with special reference to the determination of surface area and porosity, *Pure Appl. Chem.* 57 (1985) 603–619, <http://dx.doi.org/10.1351/pac198557040603>.
- [44] J.C. Groen, L.A. Peffer, J. Pérez-Ramírez, Pore size determination in modified micro- and mesoporous materials. Pitfalls and limitations in gas adsorption data analysis, *Microporous Mesoporous Mater.* 60 (2003) 1–17, [http://dx.doi.org/10.1016/S1387-1811\(03\)00339-1](http://dx.doi.org/10.1016/S1387-1811(03)00339-1).
- [45] C.-J. Jia, M. Schwickardi, C. Weidenthaler, W. Schmidt, S. Korhonen, B.M. Weckhuysen, F. Schüth, Co₃O₄-SiO₂ nanocomposite: a very active catalyst for CO oxidation with unusual catalytic behavior, *J. Am. Chem. Soc.* 133 (2011) 11279–11288, <http://dx.doi.org/10.1021/ja2028926>.
- [46] Z. Ren, Y. Guo, Z. Zhang, C. Liu, P.-X. Gao, Nonprecious catalytic honeycombs structured with three dimensional hierarchical Co₃O₄ nano-arrays for high performance nitric oxide oxidation, *J. Mater. Chem. A* 1 (2013) 9897, <http://dx.doi.org/10.1039/c3ta11156c>.
- [47] V.G. Hadjiev, M.N. Iliev, I.V. Vergilov, The Raman spectra of Co₃O₄, *J. Phys. C Solid State Phys.* 21 (1988) L199–L201, <http://dx.doi.org/10.1088/0022-3719/21/7/007>.
- [48] G. Wang, X. Shen, J. Horvat, B. Wang, H. Liu, D. Wexler, J. Yao, Hydrothermal synthesis and optical, magnetic, and supercapacitance properties of nanoporous cobalt oxide nanorods, *J. Phys. Chem. C* 113 (2009) 4357–4361, <http://dx.doi.org/10.1021/jp8106149>.
- [49] T. Yu, Y. Zhu, X. Xu, Z. Shen, P. Chen, C.T. Lim, J.T.L. Thong, C.H. Sow, Controlled growth and field-emission properties of cobalt oxide nanowalls, *Adv. Mater.* 17 (2005) 1595–1599, <http://dx.doi.org/10.1002/adma.200500322>.
- [50] J. Yang, H. Liu, W.N. Martens, R.L. Frost, Synthesis and characterization of cobalt hydroxide, cobalt oxyhydroxide, and cobalt oxide nanodiscs, *J. Phys. Chem. C* 114 (2010) 111–119, <http://dx.doi.org/10.1021/jp908548f>.
- [51] Z. Nickolov, G. Georgieva, D. Stoilovab, I. Ivanova, Raman and IR study of cobalt acetate dihydrate, *J. Mol. Struct.* 354 (1995) 119–125.
- [52] A. Rezaeifard, R. Haddad, M. Jafarpour, M. Hakimi, Catalytic epoxidation activity of keplerate polyoxomolybdate nanoball toward aqueous suspension of olefins under mild aerobic conditions, *J. Am. Chem. Soc.* 135 (2013) 10036–10039, <http://dx.doi.org/10.1021/ja405852s>.
- [53] A.S. Hay, H.S. Blanchard, Autoxidation reactions catalyzed by cobalt acetate bromide, *Can. J. Chem.* 43 (1965) 1306–1317, <http://dx.doi.org/10.1139/v65-178>.
- [54] A. Shilov, G. Shul'pin, Homogeneous catalytic oxidation of hydrocarbons by molecular oxygen, *Act. Catal. React. Satur. Hydrocarb. Presence Met. Complex.* (2002) 371–429, http://dx.doi.org/10.1007/0-306-46945-6_10.
- [55] H.C. Brown, Y. Okamoto, Electrophilic substituent constants, *J. Am. Chem. Soc.* 80 (1958) 4979–4987, <http://dx.doi.org/10.1021/ja01551a055>.
- [56] C.D. Johnson, *The Hammett Equation*, CUP Arch., 1973.
- [57] C. Hansch, a Leo, R.W. Taft, A survey of Hammett substituent constants and resonance and field parameters, *Chem. Rev.* 91 (1991) 165–195, <http://dx.doi.org/10.1002/chin.199139332>.
- [58] K.J. Laidler, The development of the Arrhenius equation, *J. Chem. Educ.* 61 (1984) 494–498, <http://dx.doi.org/10.1021/ed061p494>.
- [59] X. Xu, J. Li, Z. Hao, CeO₂-Co₃O₄ catalysts for CO oxidation, *J. Rare Earths* 24 (2006) 172–176, [http://dx.doi.org/10.1016/S1002-0721\(06\)60088-4](http://dx.doi.org/10.1016/S1002-0721(06)60088-4).
- [60] Z. Fei, S. He, L. Li, W. Ji, C.-T. Au, Morphology-directed synthesis of Co₃O₄ nanotubes based on modified Kirkendall effect and its application in CH₄ combustion, *Chem. Commun.* 48 (2012) 853, <http://dx.doi.org/10.1039/c1cc15976c>.
- [61] T.S. Glazneva, N.S. Kotsarenko, E.A. Kotsarenko, Surface acidity and basicity of oxide catalysts: from aqueous suspensions to in situ measurements, *Kinet. Catal.* 49 (2008) 859–867, <http://dx.doi.org/10.1134/S0023158408060104>.
- [62] S. Mandal, A. Sinhamahapatra, B. Rakesh, R. Kumar, A. Panda, B. Chowdhury, Synthesis, characterization of Ga-TUD-1 catalyst and its activity towards styrene epoxidation reaction, *Catal. Commun.* 12 (2011) 734–738, <http://dx.doi.org/10.1016/j.catcom.2011.01.004>.
- [63] F. Lin, R. Delmelle, T. Vinodkumar, B.M. Reddy, A. Wokaun, I. Alkneit, Correlation between the structural characteristics, oxygen storage capacities and catalytic activities of dual-phase Zn-modified ceria nanocrystals, *Catal. Sci. Technol.* 5 (2015) 3556–3567, <http://dx.doi.org/10.1039/C5CY00351B>.
- [64] J. Liang, Q. Zhang, H. Wu, G. Meng, Q. Tang, Y. Wang, Iron-based heterogeneous catalysts for epoxidation of alkenes using molecular oxygen, *Catal. Commun.* 5 (2004) 665–669, <http://dx.doi.org/10.1016/j.catcom.2004.08.010>.
- [65] Q. Tang, Q. Zhang, H. Wu, Y. Wang, Epoxidation of styrene with molecular oxygen catalyzed by cobalt(II)-containing molecular sieves, *J. Catal.* 230 (2005) 384–397, <http://dx.doi.org/10.1016/j.jcat.2004.12.017>.
- [66] D. Qian, H. Hu, F. Liu, B. Tang, W. Ye, Y. Wang, J. Zhang, Gold I-catalyzed highly diastereo- and enantioselective alkyne oxidation/cyclopropanation of 1, 6-enynes, *Angew. Chem. Int. Ed.* 53 (2014) 13751–13755, <http://dx.doi.org/10.1002/anie.201407717>.
- [67] W. Ren, J. Liu, L. Chen, X. Wan, Ruthenium-catalyzed alkyne oxidation with part-per-million catalyst loadings, *Adv. Synth. Catal.* 352 (2010) 1424–1428, <http://dx.doi.org/10.1002/adsc.201000250>.
- [68] L. Zhang, A non-diazo approach to α -oxo gold carbenes via gold-catalyzed alkyne oxidation, *Acc. Chem. Res.* 47 (2015) 877–888.
- [69] K. Fukui, T. Yonezawa, C. Nagata, Theory of substitution in conjugated molecules, *Bull. Chem. Soc. Jpn.* 27 (1954) 423–427, <http://dx.doi.org/10.1246/bcsj.27.423>.
- [70] T. Pruiß, D.J. Macquarrie, J.H. Clark, Pyridine-4-ylmethyl-propyl-amine-organo-modified HMS as support for in situ formed cobalt complexes – influence of the metal source on structure and catalytic activity in the aerial epoxidation of olefins, *Appl. Catal. A Gen.* 276 (2004) 29–37, <http://dx.doi.org/10.1016/j.apcata.2003.12.001>.
- [71] R. Hernández Sánchez, S.L. Zheng, T.A. Betley, Ligand field strength mediates electron delocalization in octahedral [(HL)₂Fe₆(L_m)_n]⁺ clusters, *J. Am. Chem. Soc.* 137 (2015) 11126–11143, <http://dx.doi.org/10.1021/jacs.5b06453>.
- [72] G. Lian, X. Zhang, M. Tan, S. Zhang, D. Cui, Q. Wang, Facile synthesis of 3D boron nitride nanoflowers composed of vertically aligned nanoflakes and fabrication of graphene-like BN by exfoliation, *J. Mater. Chem.* 21 (2011) 9201, <http://dx.doi.org/10.1039/c0jm04503a>.
- [73] C. Pulla Rao, A. Muralikrishna Rao, C.N.R. Rao, Crystal and molecular structures of alkali- and alkaline-earth-metal complexes of N, N-dimethylformamide, *Inorg. Chem.* 23 (1984) 2080–2085, <http://dx.doi.org/10.1021/ic00182a020>.
- [74] S. Rahman, S.A. Farooqui, A. Rai, R. Kumar, C. Santra, V.C. Prabhakaran, G.R. Bhadu, D. Sen, S. Mazumder, S. Maity, A.K. Sinha, B. Chowdhury, Mesoporous TUD-1 supported indium oxide nanoparticles for epoxidation of styrene using molecular O₂, *RSC Adv.* 5 (2015) 46850–46860, <http://dx.doi.org/10.1039/C5RA03400K>.
- [75] Y. Liang, C. Yi, S. Tricard, J. Fang, J. Zhao, W. Shen, Prussian blue analogues as heterogeneous catalysts for epoxidation of styrene, *RSC Adv.* 5 (2015) 17993–17999, <http://dx.doi.org/10.1039/C4RA16570E>.